Eur. Phys. J. B **47**, 207–211 (2005)
DOI: 10.1140/epjb/e2005-00316-y

**THE EUROPEAN PHYSICAL JOURNAL B**

# Temperature dependence of phase separation and magnetic anisotropy by electron spin resonance in $Pr_{0.6}Ca_{0.4}Mn_{0.9}Ru_{0.1}O_3$

C. Autret-Lambert[1,a], M. Gervais[1], M. Zaghrioui[1], S. Roger[1], F. Gervais[1], N. Raimboux[2], and P. Simon[2]

[1] LEMA, UMR 6157 CNRS-CEA, Faculté des Sciences et Techniques, Université François Rabelais, Parc de Grandmont, 37200 Tours, France
[2] CRMHT, UPR4212 CNRS, 45071 Orléans Cedex 02, France

Received 4 February 2005 / Received in final form 13 July 2005
Published online 11 October 2005 – 

**Abstract.** Electron spin resonance (ESR) measurements have been performed on polycrystalline samples of $Pr_{0.6}Ca_{0.4}Mn_{1-x}Ru_xO_3$ ($x = 0, 0.1$). The substitution of Ru in the Mn-site strengthens ferromagnetic interactions due to the double exchange between the $Mn^{3+}$ and $Mn^{4+}$ species and super-exchange between the $Ru^{5+}$ and $Mn^{3+}$ species. The temperature dependence of the ESR spectra indicates development of magnetic phase separation in $Pr_{0.6}Ca_{0.4}Mn_{0.9}Ru_{0.1}O_3$ in contrast with the un-doped sample.

**PACS.** 75.47.Lx Manganites – 75.30.Gw Magnetic anisotropy – 76.50.+g Ferromagnetic, antiferromagnetic, and ferrimagnetic resonances; spin-wave resonance

## Introduction

Manganite perovskites ($Ln_{1-x}AE_xMnO_3$, where AE is a divalent alkaline-earth, Ln is a trivalent lanthanide and $x$ the doping concentration) show many interesting phenomena [1]. In the past 15 years, the discovery of colossal magnetoresistance (CMR) has renewed interest in this kind of material [2,3]. More recently, many studies revealed a complex phase diagram, for example paramagnetic insulator (PMI), ferromagnetic insulator (FMI), ferromagnetic metallic (FMM) and antiferromagnetic insulator (AFMI), but also charge order (CO), orbital order (OO) and Jahn-Teller effect [4,5].

The basic mechanism in CMR manganites is generally double exchange (DE) interaction, i.e. the existence of strong FM interactions between $Mn^{3+}$ and $Mn^{4+}$ species [6]. However, the AFMI phase is expected to play a very important role in the appearance of the CMR properties. It has been shown that the electronic phase separation scenario leads to CMR effect [7,8]. This scenario consists in the competition between the FMM and antiferromagnetic insulator (AFMI) ground states. For small A-site cations, the compounds exhibit an AFM phase at low temperature, CE-type in the Wollan and Koehler notation, which is associated with charge ordering [9,10]. Under magnetic field or pressure, the CO state can transform into a FMM state. The intensity of the required magnetic field was shown to decrease with the increase of average size of A-site cation $\langle r_A \rangle$ [11]. Recently, it has been shown that the substitution of Mn by various cations can induce metallicity and ferromagnetism even in the absence of a magnetic field [12]. Whatever the nature of AFM, the introduction of magnetic cation on the Mn site leads to an effect similar to that obtained with an external magnetic field. The substitution of foreign cations may induce the collapse of orbital and charge ordering, and the development of ferromagnetic clusters around the doping element, leading to phase separation [13]. Among the magnetic cations, Ru is a good candidate to induce metallicity and ferromagnetism, because the large size of $Ru^{4+}$ compared with $Mn^{4+}$ induces an internal pressure effect and also because of its ability to adopt two valences $Ru^{4+}$ and $Ru^{5+}$. On the one hand the creation of $Mn^{3+}$ when $Ru^{5+}$ replaces $Mn^{4+}$ leads to the development of DE between $Mn^{3+}$ and $Mn^{4+}$ species. On the other hand, they can both participate to strong super-exchange FM interactions with $Mn^{3+}$ [14–16].

Among the experiments able to evidence local magnetic order, electron magnetic resonance (EMR) is worth considering, namely electron paramagnetic resonance (EPR) in the paramagnetic domain and ferromagnetic (or antiferromagnetic) resonance (FMR or AFMR) below the Curie temperature ($T_C$) (or below the Néel temperature $T_N$). This technique is helpful for understanding magnetic interactions and spin correlations. Few groups focused studies on the phase separation manganites by ferromagnetic resonance investigations [17–19]. They show the coexistence of FMI and FMM below $T < T_C$ and

[a] e-mail: cecile.autret@univ-tours.fr

the presence of FM clusters embedded into the PM matrix above this temperature [20]. In an EMR spectrum, the resonance of Mn gives a single line near $g = 2$ in a paramagnetic or antiferromagnetic phase, whereas in a ferromagnetic phase, the line is shifted to low fields, what constitutes an unambiguous signature of FM phase. On the other hand, PM and AFM behaviours are discriminated from the temperature dependence of linewidth. This protocol promotes EMR spectroscopy to probe phase separation phenomena.

An ESR study was carried out for one polycrystalline sample $Pr_{0.6}Ca_{0.4}Mn_{0.9}Ru_{0.1}O_3$ compared with the undoped compound, $Pr_{0.6}Ca_{0.4}MnO_3$ in connection with the magnetic measurements. It includes the temperature dependence of ESR spectra and the evidence for magnetic inhomogeneities.

## Experiments

Polycrystalline samples were prepared by an organic gel-assisted citrate process. The gel obtained was calcined at 750 °C for 5 h to give an intermediate black powder. The mixed powder was pressed into pellets and heated at 1250 °C in air, held at this temperature for a period of 12 h and then cooled down to room temperature. Scanning electron microscopy (SEM, Zeiss DSM 982) in the secondary electron emission mode was used to evaluate the surface microstructure. Two representative SEM micrographs are shown in Figure 1. The average grain size was evaluated indeed around 1 $\mu$m but there is a large distribution of grain size. The cationic composition was investigated by energy dispersive X-ray spectroscopy (EDS) analysis. The EDS analysis showed a nearly homogeneous composition of the compounds in agreement with the nominal composition ($Pr_{0.6}Ca_{0.4}Mn_{0.9}Ru_{0.1}O_3$). The powder X-ray diffraction patterns were recorded at room temperature by using a D8 diffractometer ($\theta - \theta$) with a Cu $K_\alpha$ radiations. The magnetic susceptibility ($\chi$) was measured with a Manics Faraday-based magnetosusceptometer in the range 80 K to 300 K under a magnetic field of 1 T. ESR studies were performed with a Bruker ER 200-SRC spectrometer and were carried out at 9.5 GHz (X-band) on the loose packed powder obtained by crushing the pellets. A very small amount of powder (≈100 $\mu$g) is sufficient and was placed at the bottom of a cavity. The studies were measured upon heating from 130 K to 370 K by step of 10 K. The temperature dependence of $g_{\text{eff}}$, calculated via $g_{\text{eff}} = h\upsilon/\mu_B H_{\text{res}}$, linewidth $\Delta H_{\text{pp}}$ and double integrated intensity (DIN) (which is proportional to the EMR susceptibility $X_{\text{EMR}}$) were analysed. The average effective value $g_{\text{eff}}$ was calculated from the resonance field (Hr) and the linewidth $\Delta H_{\text{pp}}$ was deduced from the peak-to-peak distance between the maximum and the minimum of the derivative of the ESR absorption.

## Results

The XRD patterns indicated a single phase with an orthorhombic symmetry of Pbnm space group characteristic of O-type $b > c/\sqrt{2} > a$, for both compounds (Fig. 2). For the un-doped compound $Pr_{0.6}Ca_{0.4}MnO_3$, the refined cell parameters are close to $a = 5.4133(2)$ Å, $b = 5.4368(2)$ Å, $c = 7.6536(3)$ Å and $V = 225.25(2)$ Å$^3$ and the reliability factors are $R_{\text{Bragg}} = 5.02\%$ and $\chi^2$ close to 1.41. For $Pr_{0.6}Ca_{0.4}Mn_{0.9}Ru_{0.1}O_3$ compound, the following reliability factors are close to $R_{\text{Bragg}} = 4.62\%$ and $\chi^2$ close to 1.36. The Ru substitution induced an increase of the cell parameters and volume corresponding to $a = 5.4251(2)$ Å, $b = 5.4625(2)$ Å, $c = 7.6649(3)$ Å and $V = 227.14(2)$ Å$^3$. This increase agrees with previous results reported in literature [21,22]. It was attributed to the preferential replacement of $Mn^{4+}$(0.530 Å) by $Ru^{5+}$(0.565 Å) according to the equation $2Mn^{4+} \rightarrow Ru^{5+} + Mn^{3+}$ [23]. It results in an increase in $Mn^{3+}$(0.645 Å) and an increase of the Mn-site average ionic radius. The predominance of the 5+ valency state of Ru among the $Ru^{5+}$ and $Ru^{4+}$ species is supported by a number of characterizations [21,22].

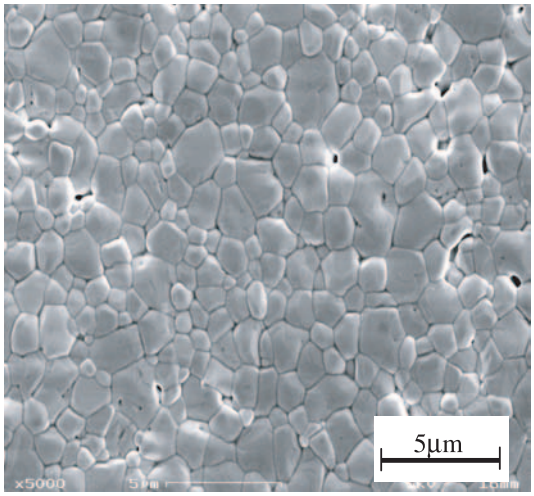


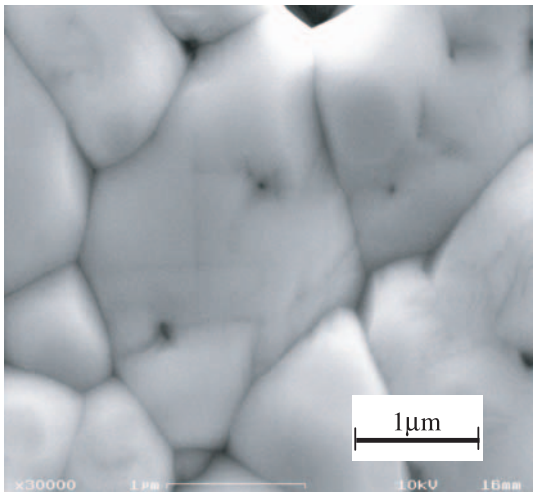


**Fig. 1.** Two typical scanning electron micrographs showing the size and the distribution of grains for $Pr_{0.6}Ca_{0.4}Mn_{0.9}Ru_{0.1}O_3$.

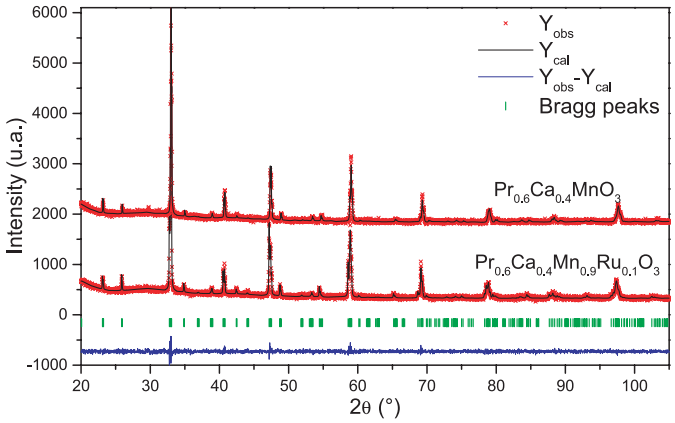


**Fig. 2.** Final refinement, with experimental (+), calculated (–) and difference X-ray powder diffraction patterns of $Pr_{0.6}Ca_{0.4}MnO_3$ ($R_{\rm Bragg}$ = 5.02%, $\chi^2$ = 1.41) and $Pr_{0.6}Ca_{0.4}Mn_{0.9}Ru_{0.1}O_3$ ($R_{\rm Bragg}$ = 4.62%, $\chi^2$ = 1.36) ($\lambda$ = 1.54 Å).

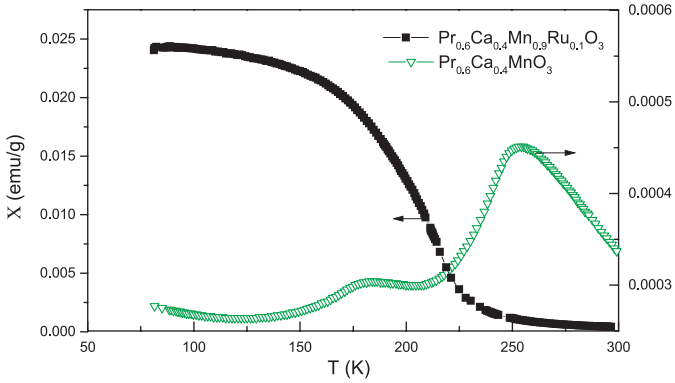


**Fig. 3.** ZFC magnetic susceptibility from 300 K to 80 K with an applied field of 1 T. For clarity, two scales were used for $Pr_{0.6}Ca_{0.4}Mn_{0.9}Ru_{0.1}O_3$ and for $Pr_{0.6}Ca_{0.4}MnO_3$.

The $\chi$(T) curves for $Pr_{0.6}Ca_{0.4}Mn_{0.9}Ru_{0.1}O_3$ and $Pr_{0.6}Ca_{0.4}MnO_3$ are shown in Figure 3. The $\chi$(T) curves for un-doped $Pr_{0.6}Ca_{0.4}MnO_3$ exhibits two bumps, one at ≈250 K and a smaller one at ≈170 K. The sharp bump at 250 K is a signature of the charge ordering transition at $T = T_{\rm CO}$. Below $T_{\rm CO}$, the large decrease of $\chi$ may be attributed to the development of an antiferromagnetic behaviour with a Néel temperature corresponding to the second bump $T_{\rm N}$ = 170 K. For the doped sample, as the temperature decreases, a large increase of $\chi$ is observed at about 220 K, which is consistent with the development of a FM phase.

Figure 4 shows ESR spectra versus temperature for the $Pr_{0.6}Ca_{0.4}MnO_3$ un-doped compound. The responses remain single line over the temperature range from 370 K down to 130 K. The evolution of $g_{\rm eff}$ and $\Delta H_{\rm pp}$ versus $T$ are shown in Figure 5. Like $Pr_{0.4}Ca_{0.6}MnO_3$ (Ref. 24), $Pr_{0.6}Ca_{0.4}MnO_3$ shows two CO and AFM states at two different temperatures. The temperature of both charge ordering and antiferromagnetic transitions were determined from the $g_{\rm eff}$ and $\Delta H_{\rm pp}$ profiles [24]. $T_{\rm CO}$ was shown to correspond to the minimum of the $\Delta$H$_{\rm pp}$ curve at 250 K.

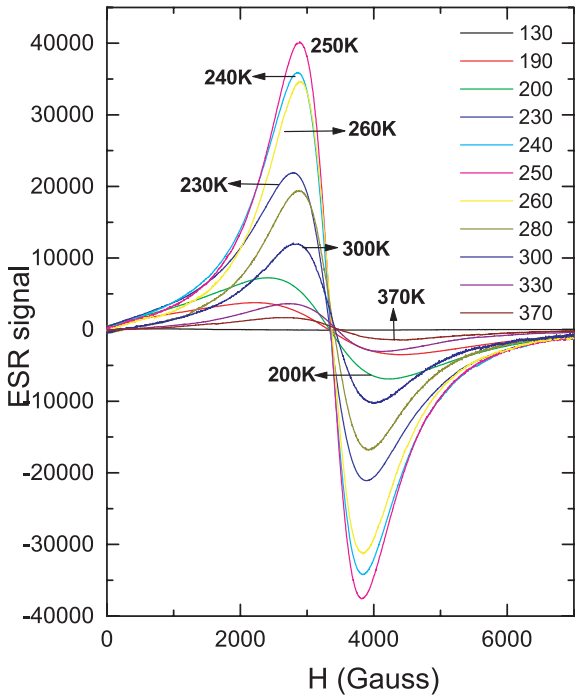


**Fig. 4.** ESR spectra of $Pr_{0.6}Ca_{0.4}MnO_3$ between 360 K and 130 K.

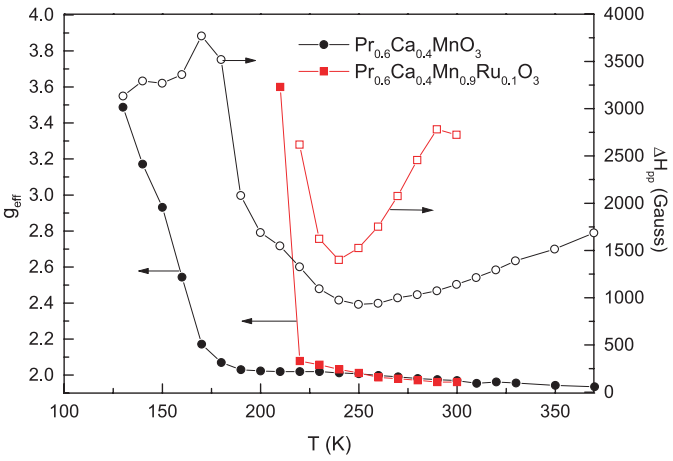


**Fig. 5.** Temperature dependence of the lineshape parameters for $Pr_{0.6}Ca_{0.4}MnO_3$ and $Pr_{0.6}Ca_{0.4}Mn_{0.9}Ru_{0.1}O_3$, $g_{\rm eff}$-factor (left $y$-axis), linewidth (right $y$-axis).

This transition does not affect $g_{\rm eff}$ that remains at a value close to 2. $T_{\rm N}$ was shown to correspond to both a maximum in the $\Delta H_{\rm pp}$ curve and to the abrupt increase of $g_{\rm eff}$, characteristic of a crossover from paramagnetic to antiferromagnetic resonance. These transitions are also observed in the susceptibility and DIN curves (Figs. 3 and 6). The ESR measurements are thus able to discriminate the charge order ($T_{\rm CO}$ = 250 K) and PM-AFM ($T_{\rm N}$ = 170 K) transitions.

The substitution of Ru on the Mn-site leads to more complex ESR spectra (Figs. 7a and 7b). In the PM regime, between about 300 and 230 K, a single Lorentzian line is observed. As the temperature decreases from 230 K,

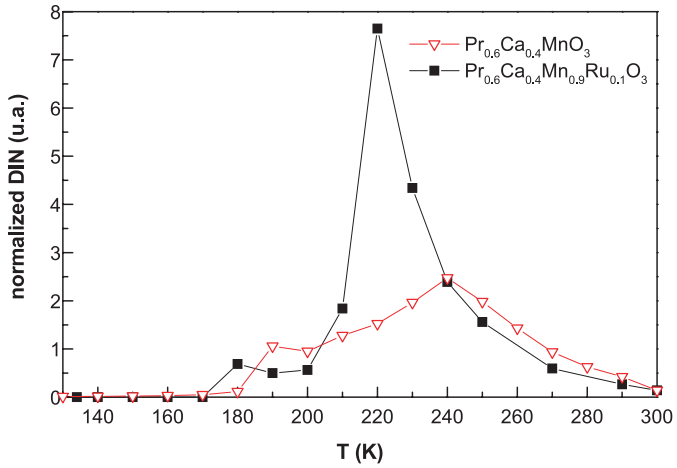


**Fig. 6.** Temperature dependences of double integrated intensities (EMR susceptibilities) for $Pr_{0.6}Ca_{0.4}MnO_3$ and $Pr_{0.6}Ca_{0.4}Mn_{0.9}Ru_{0.1}O_3$ normalized to those at $T = 300$ K.

the peak broadens and shifts towards lower fields. This is a characteristic of the appearance of a FM phase [24]. The shift is caused by the crossover to ferromagnetic resonance, where the line position is mainly governed by magneto-crystalline anisotropy [25]. At 220 K, an additional peak can be observed on the high field side near $g = 2$ (Hr = 3500 G), attributed to the presence of some remaining PM phase. So, the transition is broad in accordance with the $\chi$(T) curve (Fig. 3). Below 210 K, the spectrum is split and lines broaden. The principal peak shifts towards lower fields and an additional peak can be observed on the high field side. A particular behaviour occurs below 190 K, the resonance field becomes very high, with a $g_{\text{eff}}$ value much smaller than 2. In single crystals, the magneto-crystalline anisotropy induces an angular dependence which may concern high fields, since the resonance field depends on the direction of the crystallographic axes with respect to the applied magnetic field [25]. The spectra are then the consequence of the superposition of single crystals in different orientations, since many poly-oriented crystallites may be agglomerated in a grain.

The temperature dependences of $g_{\text{eff}}$ and $\Delta H_{\text{pp}}$ between about 300 and 210 K are shown in Figure 5. At room temperature, both compounds $Pr_{0.6}Ca_{0.4}MnO_3$ and $Pr_{0.6}Ca_{0.4}Mn_{0.9}Ru_{0.1}O_3$ are in the paramagnetic phase. $\Delta H_{\text{pp}}$ value is higher for $Pr_{0.6}Ca_{0.4}Mn_{0.9}Ru_{0.1}O_3$ (Fig. 5) and confirms that Ru substitutes the Mn sites in agreement with the evolution of the cell parameters. This increase of $\Delta H_{\text{pp}}$ has been explained by the increase of spin-spin interactions between localized $Mn^{4+}$ and $Ru^{5+}$ carrier species which tends to broaden the ESR response [26]. For the un-doped compound, the $\Delta H_{\text{pp}}$(T) curves show a minimum at about 250 K and a maximum at 170 K corresponding to $T_{\text{CO}}$ and $T_{\text{N}}$ respectively [24]. For $Pr_{0.6}Ca_{0.4}Mn_{0.9}Ru_{0.1}O_3$, $g_{\text{eff}}$ remains nearly constant and close to 2 down to 220 K and then increases rapidly. As the temperature decreases, $\Delta H_{\text{pp}}$ decreases in a quasi-linear regime of temperature, goes through a minimum at $T_{\text{min}} = 240$ K and then increases. The variations of both $g_{\text{eff}}$ and $\Delta H_{\text{pp}}$ are consistent with a PM-FM

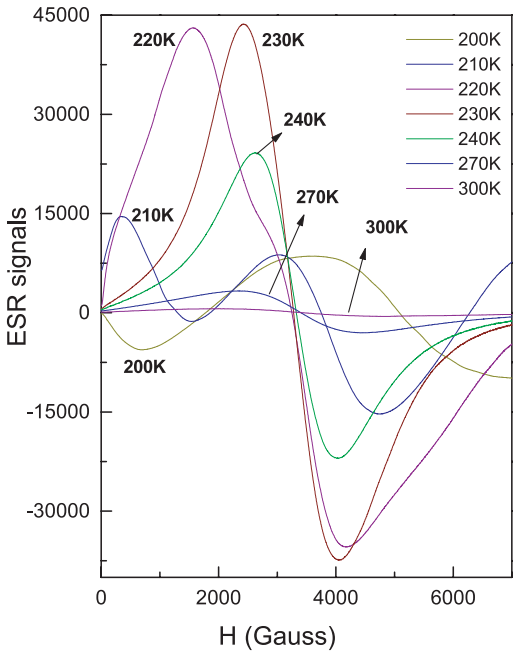


(a)

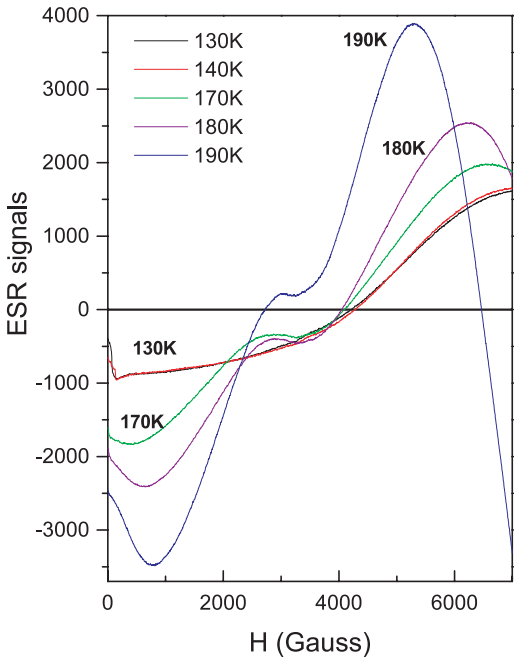


(b)

**Fig. 7.** (a) ESR spectra of the $Pr_{0.6}Ca_{0.4}Mn_{0.9}Ru_{0.1}O_3$ from 200 K to 300 K. For clarity, the spectra from 130 K up to 190 K are in (b).

transition [24]. In the temperature dependence of $\Delta H_{\text{pp}}$, $T(\Delta H_{\text{min}})$ is close to $\approx 1.1 T_{\text{C}}$ ($Tc \approx 220$ K) and corresponds to the deviation of the spectrum from Lorentzian line shape [17,19,24]. This is attributed to the existence of magnetic inhomogeneity, which is created by the appearance of FM phase within the PM matrix. Between $T_{\text{C}}$ and $T(\Delta H_{\text{min}})$, the application of a high field could

induce a partial alignment of the Mn spins along the field direction. Some of them are concentrated into small domains (or clusters) with short range FM coupling. This is why the line broadens and this leads to magnetic heterogeneity. Double integrated intensities (DIN) temperature dependence for both doped and un-doped samples are compared in Figure 6. The DIN evolutions are significantly different. For the un-doped sample, the DIN plot allows to retrieve the transition temperatures $T_{CO}$ and $T_N$ previously evidenced. The DIN plot obtained for the doped samples exhibits a sharp maximum at 220 K corresponding to the FM transition and a smaller maximum at 180 K. This bump is close to the AFM transition of the un-doped compound. It can be related to the shoulder occurring at about 3500 G for all the ESR spectra at temperatures under about 190 K. The presence of an AFM phase at $T < 180$ K can be correlated with the small value of $\chi$ (1.66 $\mu_B$/Mn at 80 K).

The DIN curve, which generally resembles the behaviour of the AC susceptibility, exhibits a double maximum for $Pr_{0.6}Ca_{0.4}Mn_{0.9}Ru_{0.1}O_3$. This feature is characteristic for mixed AFM-FM system, i.e. phase separation ground state below $T_N$, consistent with $\chi(T)$ which exhibits FM interactions down to 80 K. This fact can be explained by Ru valency effect and consequently Mn valency. Moreover, taking account of the AFM interactions in the un-doped compound, AFM super-exchange between Mn and Ru species operates also in $Pr_{0.6}Ca_{0.4}Mn_{0.9}Ru_{0.1}O_3$. As a result of Ru doping, a phase separated state is developed, with two magnetic states: AFM and FM, with the Curie temperature higher than the Néel temperature. The ESR and susceptibility studies demonstrate a drastic difference between both compounds showing AFM and mixed ground state. It is shown that the valency effect of Ru doping plays a crucial role in the appearance of the phase separation of AFM and FM states.

## Conclusion

$\chi$(T) and ESR measurements were carried out on $Pr_{0.6}Ca_{0.4}Mn_{0.9}Ru_xO_3$ ($x$ = 0, 0.1) in the temperature interval 300–100 K. Results indicate that Ru doping leads to the disappearance of charge ordering, coupled with the appearance of ferromagnetism with $T_c$ at about 220 K. The onset of ferromagnetism is related to the valency effect of Ru on the $Mn^{4+} \Leftrightarrow Mn^{3+}$ double exchange and to additional FM interactions between Ru and Mn species through superexchange [22]. The temperature dependence of $\chi$ is consistent with the presence of a ferromagnetic phase down to 80 K. The high sensitivity of ESR to both minor magnetic phases and short range interactions allows to detect the presence of an AF phase for temperatures lower than $T_N$ = 180 K. The experimental results suggest the development of an inhomogeneous ground state (AFM + FM) for temperatures lower about 180 K.

The authors thank P.Y. Sizaret and B. Arbeille for the scanning electron microscopy measurements.

## References

1. G.H. Jonker, J.H. Van Santen, Physics **16**, 337 (1950)
2. S. Jin, T.H. Tiefel, M. McCormack, R.R. Fastnatch, R. Ramesh, L.H. Chen, Science **264**, 413 (1994)
3. R. Von Helmot, J. Wecker, B. Holzapfel, L. Schultz, K. Samwer, Phys. Rev. Lett. **71**, 2331 (1994)
4. *Colossal magnetoresistance charge ordering and related properties of manganese oxides*, edited by C.N.R. Rao, B. Raveau (World Scientific, Singapore, 1998)
5. E. Dagotto, T. Hotta, A. Moreo, Phys. Rep. **344**, 1 (2001)
6. C. Zener, Phys. Rev. **82**, 403 (1951)
7. A. Moreo, S. Yunoki, E. Dagotto, Science **283**, 2034 (1999)
8. M. Uehara, S. Mori, C.H. Chen, S.W. Cheong, Nature **399**, 560 (1999)
9. E.O. Wollan, W.C. Koehler, Phys. Rev. **100**, 545 (1955)
10. Z. Jirak, S. Krupicka, Z. Simsa, M. Dhoula, S. Vratislav, J. Magn. Magn. Mater. **53**, 153 (1985)
11. Y. Tokura, Y. Tomioka, J. Magn. Magn. Mater. **200**, 1 (1999)
12. B. Raveau, A. Martin, A. Maignan, J. Solid State Chem. **130**, 162 (1997)
13. T. Kimura, Y. Tomioka, R. Kumai, Y. Okimoto, Y. Tokura, Phys. Rev. Lett. **83**, 3940 (1999)
14. P.V. Vanitha, A. Arulraj, C.N.R. Rao, C. R. Acad. Sci. Paris, série IIc, 595 (1999)
15. C. Martin, A. Maignan, M. Hervieu, C. Autret, B. Raveau, D.I. Khomskii, Phys. Rev. B **63**, 174402 (2001)
16. B. Raveau, A. Maignan, C. Martin, R. Mahendiran, M. Hervieu, J. Solid State Chem. **151**, 330 (2000)
17. S.E. Lofland, S.M. Baghat, H.L. Ju, G.C. Xiong, T. Venkatesan, R.L. Greene, Phys. Rev. B **52**, 15058 (1995)
18. A.I. Shames, E. Rozenberg, W.H. McCarroll, M. Greenblatt, G. Gorodetsky, Phys. Rev. B **64**, 172401 (2001)
19. A.I. Shames, E. Rozenberg, G. Gorodetsky, A.A. Arsenov, D.A. Shulyatev, Ya.M. Mukovskii, A. Gedanken, G. Pang, J. Appl. Phys. **91**, 7929 (2002)
20. V. Markovich, E. Rozenberg, A.I. Shames, G. Gorodetsky, I. Fita, K. Suzuki, R. Puzniak, D.A. Shulyatev, Ya.M. Mukovskii, Phys. Rev. B **65**, 144402 (2002)
21. L. Pi, S. Hébert, C. Martin, A. Maignan, B. Raveau, Phys. Rev. B **67**, 024430 (2004)
22. V. Markovich, I. Fita, R. Puzniak, E. Rozenberg, C. Martin, A. Wisniewski, A. Maignan, B. Raveau, Y. Yuzhelevskii, G. Gorodestky, Phys. Rev. B **70**, 024403 (2004)
23. D. Shannon, Acta Cryst. A, **32**, 751 (1976)
24. C. Autret, M. Gervais, F. Gervais, N. Raimboux, P. Simon, Solid State Sci. **6**, 815 (2004)
25. S. Angappane, M. Pattabiraman, G. Rangarajan, K. Sethupathi, V.S. Sastry, Phys. Rev. B **69**, 094437 (2004)
26. A.I. Shames, E. Rozenberg, C. Martin, A. Maignan, B. Raveau, G. André, G. Gorodestsky, Phys. Rev. B **70**, 134433 (2004)